ADVANCED MATERIALS

trate (GNO, Alfa Aesar, Ward Hill, MA) for 6 h at 16 °C. The products were collected and washed by centrifugation before analysis. For reactions at low concentration, native and denatured filaments at 0.2 mg mL^{-1} were incubated in 1.6 mL polyethylene centrifuge tubes with 1 mL of a 0.1 M aqueous solution of gallium nitrate for 24 h at 25 °C. The products were collected and washed by centrifugation before analysis. Base-catalyzed synthesis of Ga_2O_3 was accomplished by dissolving 1.82 g (0.005 mol) of GNO in 30 g of water contained in a glass vessel, followed by the addition of 7.24 g (0.06 mol) of concentrated (~29 wt.-%) ammonium hydroxide (NH_4OH). Precipitated product was collected and washed by centrifugation before heat treatment. Hydrated GNO was prepared by dissolving 1.82 g (0.005 mol) of GNO in 50 g of water contained in a glass vessel. The solution was mixed for 1 h, followed by room-temperature vacuum evaporation of the water. The dried powder product was used for further heat treatments. As-received GNO powder was used directly from the container for pyrolysis experiments. Thermal treatments of base-hydrolyzed, hydrated, and as-received GNO powders were conducted by heating 50 mg of starting material in alumina crucibles placed in quartz Schlenk tubes. Heat treatments (10 °C min^{-1}) were carried out in air to temperatures between 200–1000 °C for 1 h.

X-ray Diffraction (XRD), Scanning Electron Microscopy (SEM), and Transmission Electron Microscopy (TEM): Approximately 25 mg of each heat-treated sample was ground (with a silicon-powder internal standard) to a fine powder, placed on a glass microscope slide or a single-crystal (100) silicon wafer, and characterized by X-ray diffraction (Phillips X'Pert; Amsterdam, The Netherlands) using a gonio scan (20°–60°, 0.02° step^{-1}, 5 s step^{-1}; source slit sizes of 1/4° and 1/2°, and detector slit sizes of 1/4° and 0.2 mm). Surface features of Ga_2O_3 powders and Ga_2O_3-coated silicatein filaments were imaged by a cold cathode field-emission scanning electron microscope (SEM; JEOL JSM 6300F, Peabody, MA) equipped with an energy dispersive spectrometer. Specimens were mounted on conductive carbon adhesive tabs (Ted Pella, Inc., Redding, CA) and imaged (at 5 kV or 10 kV) either uncoated (for energy dispersive spectroscopy analysis) or after gold/palladium sputter coating. Energy dispersive spectroscopy (EDS, Oxford Instruments, Palo Alto, CA) was performed in conjunction with SEM to qualitatively determine chemical composition of specimens. Ga_2O_3-coated filaments were imaged with a transmission electron microscope (TEM, JEOL 2000FX) to observe the coating morphologies and obtain structural information via electron diffraction patterns. Lattice fringes were imaged with a high-resolution TEM (HRTEM, JEOL 2010). Both TEMs were operated at 200 kV. TEM specimens were prepared by pipetting a small amount (~20 μL) of filament suspension (in water) onto holey-carbon copper grids (Ted Pella, Inc., Redding, CA). The grids were then dried at 40 °C for 5 min. Samples were imaged at magnifications from 20 000× to 200 000× in the conventional TEM, and from 500 000× to 800 000× in the HRTEM. Selected area electron diffraction (SAED) patterns were obtained at camera distances of 55 cm, 83 cm, and 100 cm. A standard evaporated-aluminum film (lattice constant = 0.4041 nm) was used as a standard to determine the exact camera constants.

Received: May 24, 2004
Final version: September 20, 2004

[1] A. H. Heuer, D. J. Fink, V. J. Laraia, J. L. Arias, P. D. Calvert, K. Kendall, G. L. Messing, J. Blackwell, P. C. Rieke, D. H. Thompson, A. P. Wheeler, A. Veis, A. I. Caplan, *Science* **1992**, *255*, 1098.
[2] S. Mann, *Nature* **1993**, *365*, 499.
[3] S. Weiner, L. Addadi, *J. Mater. Chem.* **1997**, *7*, 689.
[4] A. M. Belcher, P. K. Hansma, G. D. Stucky, D. E. Morse, *Acta Mater.* **1998**, *46*, 733.
[5] D. E. Morse, *Trends Biotechnol.* **1999**, *17*, 230.
[6] S. Mann, *Biomineralization: Principles and Concepts in Bioinorganic Materials Chemistry*, Oxford University Press, New York **2001**, pp. 16–23.
[7] M. Sarikaya, C. Tamerler, A. K. Y. Jen, K. Schulten, F. Baneyx, *Nat. Mater.* **2003**, *2*, 577.
[8] J. Aizenberg, D. A. Muller, J. L. Grazul, D. R. Hamann, *Science* **2003**, *299*, 1205.
[9] K. Shimizu, J. Cha, G. D. Stucky, D. E. Morse, *Proc. Natl. Acad. Sci. USA* **1998**, *95*, 6234.
[10] J. N. Cha, K. Shimizu, Y. Zhou, S. C. Christiansen, B. F. Chmelka, G. D. Stucky, D. E. Morse, *Proc. Natl. Acad. Sci. USA* **1999**, *96*, 361.
[11] Y. Zhou, K. Shimizu, J. N. Cha, G. D. Stucky, D. E. Morse, *Angew. Chem. Int. Ed.* **1999**, *38*, 779.
[12] J. L. Sumerel, W. Yang, D. Kisailus, J. C. Weaver, D. E. Morse, *Chem. Mater.* **2003**, *15*, 4804.
[13] G. Dodson, A. Wlodawer, *Trends Biochem. Sci.* **1998**, *23*, 347.
[14] D. E. Morse, in *The Chemistry of Organic Silicon Compounds*, Vol. 3 (Eds: Z. Rappoport, Y. Apeloig), Wiley, New York **2001**, pp. 805–819.
[15] J. N. Cha, G. D. Stucky, D. E. Morse, T. J. Deming, *Nature* **2000**, *403*, 289.
[16] Y. C. Choi, W. S. Kim, Y. S. Park, S. M. Lee, D. J. Bae, Y. H. Lee, G. S. Park, W. B. Choi, N. S. Lee, J. M. Kim, *Adv. Mater.* **2000**, *12*, 746.
[17] M. Ogita, K. Higo, Y. Nakanishi, Y. Hatanaka, *Appl. Surf. Sci.* **2001**, *175–176*, 721.
[18] J. Livage, M. Henry, C. Sanchez, *Prog. Solid State Chem.* **1988**, *18*, 259.
[19] J. C. Brinker, G. W. Scherer, *Sol–Gel Science: The Physics and Chemistry of Sol-Gel Processing*, Academic, Boston, MA **1990**.
[20] A. C. Tas, P. J. Majewski, F. Aldinger, *J. Am. Ceram. Soc.* **2002**, *85*, 1421.
[21] L. Loffler, W. Mader, *Am. Mineral.* **2001**, *86*, 293.
[22] R. Roy, V. G. Hill, E. F. Osborn, *J. Am. Chem. Soc.* **1952**, *74*, 719.
[23] F. C. Meldrum, B. R. Heywood, S. Mann, *Science* **1992**, *257*, 522.
[24] I. I. Yaacob, A. C. Nunes, A. Bose, *J. Colloid Interface Sci.* **1995**, *171*, 73.
[25] G. Erwin, *Acta Crystallogr.* **1952**, *5*, 103.
[26] R. McPherson, *J. Mater. Sci.* **1973**, *8*, 851.
[27] C. G. Levi, V. Jayaran, J. J. Valencia, R. Mehrabian, *J. Mater. Res.* **1988**, *3*, 969.
[28] H. Colfen, S. Mann, *Angew. Chem. Int. Ed.* **2003**, *42*, 2350.
[29] *Epitaxial Growth* (Ed: J. W. Matthews), Academic, New York **1975**.

pH-Triggered Thermally Responsive Polymer Core–Shell Nanoparticles for Drug Delivery**

By *Kumaresh S. Soppimath*, *Darren Cherng-Wen Tan*, and *Yi-Yan Yang**

Polymeric core–shell nanoparticles have emerged recently as promising colloidal carriers for targeting poorly water-soluble and amphiphilic drugs, as well as genes, to tumor tissues.[1–3] Using these nanoparticles, drug targeting can be

[*] Dr. Y.-Y. Yang, Dr. K. S. Soppimath, Dr. D. C.-W. Tan
Institute of Bioengineering and Nanotechnology
31 Biopolis way, The Nanos, 04-01, 138669 (Singapore)
E-mail: yyyang@ibn.a-star.edu.sg

[**] This work was funded by Institute of Bioengineering and Nanotechnology, Agency for Science, Technology and Research, Singapore. Supporting Information is available online from Wiley InterScience or from the author.

  DOI: 10.1002/adma.200401057

achieved either passively, through an enhanced permeation and retention effect,[4] or actively, by the incorporation of recognition signals onto the surface of the nanoparticles,[5] and by using a polymer sensitive to the surrounding temperature or pH. Core–shell nanoparticles with shells constructed from temperature-sensitive poly(*N*-isopropylacrylamide) (PNIPAAm) or its copolymers have attracted special attention because of their thermal responsiveness. PNIPAAm exhibits a lower critical solution temperature (LCST) of approximately 32 °C in aqueous solution, below which the polymer is water-soluble and above which they become water-insoluble. As such, the core–shell nanoparticles that were self-assembled from hydrophobically modified PNIPAAm polymers were stable below the LCST, but deformed at temperatures higher than the LCST because of loss of the hydrophobicity/hydrophilicity balance of the core–shell structure. Using core–shell nanoparticles having an LCST slightly higher than nominal body temperature, drug delivery may be controlled by superficially heating and cooling the local environment of the nanoparticles.[6] However such a system suffers from the disadvantage of not being easily accessible to deep organs or tumors. An alternative approach to targeting drugs to tumor tissues is to use pH-sensitive carriers. The extracellular pH in most solid tumor tissues ranges from 5.7 to 7.8,[7] with the pH of the tumor interstitial fluid rarely below pH 6.5. It is a challenging task to develop a system capable of responding to such a narrow window of pH change.[8] Recently, the core–shell nanoparticles made from poly(L-histidine)-*block*-poly(ethylene glycol) (PEG) were reported to dissociate at pH 7.0 to 7.4, thereby releasing the enclosed doxorubicin.[9,10] The dissociation of the core–shell structure was attributed to the protonation of the poly(L-histidine) block. In this study, we synthesized novel core–shell nanoparticles self-assembled from the amphiphilic tercopolymer poly(*N*-isopropylacrylamide-*co*-*N*,*N*-dimethylacrylamide-*co*-10-undecenoic acid) [P(NIPAAm-*co*-DMAAm-*co*-UA)], in which 10-undecenoic acid was employed as the hydrophobic and pH-sensitive segment. Interestingly, the temperature responsiveness of the core–shell nanoparticles can be triggered by a change in the environmental pH. The nanoparticles were stable in media of pH 7.4 at 37 °C, but dissociated and released the enclosed drug molecules in an acidic environment. Furthermore, the shell of these nanoparticles was built with amine groups, providing the possibility for the conjugation of biological signals with specific affinities to certain cell types. This would double the targeting ability of the nanoparticles. More importantly, the shell of the nanoparticles became hydrophobic in acidic environments due to the decrease of the LCST to a value below the nominal body temperature. This may improve the adhesion of the nanoparticles to tissues where the environment is characteristically acidic.[11] The polymeric core–shell nanoparticles developed would make a promising carrier for delivering drugs to acidic tumor tissues or cell interiors.

The LCST of PNIPAAm can be increased to a temperature slightly higher than the nominal body temperature by introducing a hydrophilic segment.[12] We have previously reported the synthesis of cholesteryl-terminated P(NIPAAm-*co*-DMAAm). Both NIPAAm and DMAAm monomers exhibited similar reactivity, and the LCST of the polymer in water was about 38 °C because of the presence of DMAAm.[13] In this study, DMAAm was also employed to adjust the LCST of the polymer. P(NIPAAm-*co*-DMAAm-*co*-UA) polymers with three different compositions, including Polymer I (the feed ratio of NIPAAm, DMAAm, and UA = 4.00:1.00:0.5), Polymer II (3.75:1.25:0.5), and Polymer III (3.50:1.50:0.5), were synthesized by radical copolymerization using the redox couple ammonium persulfate (APS) and 2-aminoethanethiol hydrochloride (AET·HCl) (Scheme 1).[14] The chemical structure of the polymers was confirmed by ^{1}H NMR (Bruker Avance 400, 400 MHz) and Fourier-transform infrared (Perkin Elmer

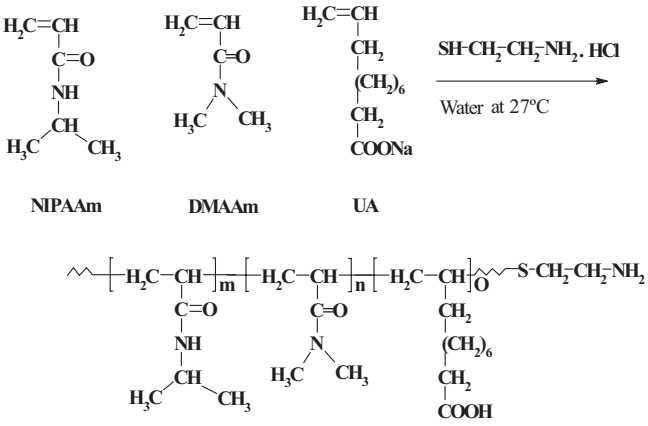

Scheme 1. Chemical synthesis route of P(NIPAAm-*co*-DMAAm-*co*-UA).

Spectrum 2000, KBr) spectroscopic methods. The actual molar ratio of NIPAAm to DMAAm was approximately equal to the feed ratio of the two monomers. The weight-average molecular weights of Polymer I, Polymer II, and Polymer III were 31, 9.3, and 11 kDa (1Da = 1.66×10^{-27} kg), respectively. The UA contents were 36.8, 44.2, and 40.5 mg per gram of polymer, respectively. The average number of amine groups in each polymer molecule was estimated to be 1.3 to 1.7 by a spectroscopic method. The polymers exhibited good solubility in both water and common organic solvents ($CHCl_3$, CH_2Cl_2, acetone, and tetrahydrofuran (THF)). The glass-transition temperatures (T_g) of the polymers were determined to be from 133 to 135 °C using a differential scanning calorimeter (TA 2920 Modulated DSC, CT, USA) with a ramp speed of 3 °C min^{-1}. Thermal analyses of the polymers, performed using a TGA 7 (Perkin Elmer, USA), showed that all the polymers had similar decomposition temperatures (T_d) ranging from 438 to 459 °C. This indicates that the polymers are thermally stable up to 400 °C. This thermal stability is an added advantage as it would mean that the polymers can be sterilized by autoclaving prior to in-vivo applications.

The LCSTs of the polymers in buffer solutions of different pH values were determined by monitoring the optical trans-

ADVANCED MATERIALS

mittance change as a function of temperature. Sample solutions (0.5 wt.-%) were prepared in buffers such as neutralized phthalate buffer (pH 5.0), phosphate-buffered saline (PBS, pH 6.0, 6.6, and 7.4), as well as in alkaline borate buffer of pH 9.0. All the buffers were prepared with an ionic strength of 154×10^{-3} M. From the results of particle-size analyses, all the three polymers in the buffer solutions self-assembled into core–shell nanoparticles at the concentration used. Optical transmittance of the core–shell nanoparticles was measured at 500 nm with a UV-vis spectrometer (UV-2501PC, Shimadzu) with the sample cell thermostated using a temperature-controller (TCC-240A, Shimadzu). The heating rate was set at $0.1\,^{\circ}\mathrm{C\,min^{-1}}$. The LCST values of the core–shell nanoparticles were determined at the temperatures showing an optical transmittance of 50 %. Table 1 lists the LCST values of the core–shell nanoparticles at different pH. An increase in the length of the hydrophilic DMAAm segment of the polymers led to an increase in the LCST under all the pH conditions

Table 1. LCSTs (° C) of the core–shell nanoparticles self-assembled from the polymers at different pH values.

Polymer	pH 5.0	pH 6.0	pH 6.6	pH 7.4	pH 9.0
Polymer I	28.9	32.8	32.7	33.1	37.7
Polymer II	35.6	36.2	35.5	38.6	40.2
Polymer III	38.7	40.7	41.0	43.0	43.2

used. The LCSTs of the core–shell nanoparticles self-assembled from Polymer I, Polymer II, and Polymer III were all pH-dependent. For instance, at pH 9.0 and 7.4, the LCSTs of Polymer II nanoparticles were found to be 40.2 and 38.6 °C, respectively, which were well above nominal body temperature (Fig. 1). However, at pH 6.6, 6.0, and 5.0, the LCSTs reduced to 35.5, 36.2, and 35.6 °C, respectively, which were

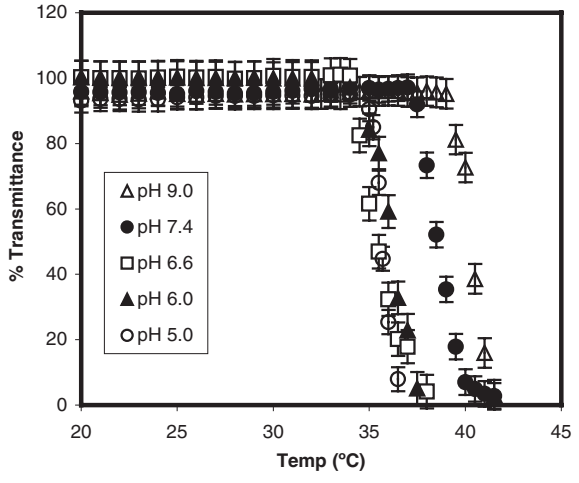

Figure 1. Plot of transmittance of Polymer II solutions as a function of temperature at varying pH at 500 nm.

much lower than nominal body temperature. If the nanoparticles have a well-separated core–shell structure, and the core is rigid enough, the LCST of the nanoparticles should not be affected by the environmental pH since the pH-sensitive moieties are in the hydrophobic segments. The core–shell nanoparticles made from these polymers may be loosely packed, thus making the core accessible to the external environment. With the increase of pH of the external environment, the carboxylic acid groups in the 10-undecenoic acid segment were more easily de-protonated, and thus reduced the hydrophobicity of the 10-undecenoic acid segment. This would lead to an increase in the LCST of the polymers, and hence, that of the nanoparticles. Compared with Polymer I and Polymer II, the temperature sensitivity of Polymer III nanoparticles was lower. This is probably due to the dilution effect of DMAAm. That is, the PNIPAAm segments in the copolymer were well separated and diluted by DMAAm segments at the high molar ratio, reducing intramolecular hydrogen bonding between neighboring amide groups of the NIPAAm. This might have accounted for the slow temperature response of the copolymer.[15] Since the blood is rich with various proteins, we have investigated the effect of proteins on the LCST of the nanoparticles using bovine serum albumin (BSA) as a model protein. The presence of 10 wt.-% BSA did not alter the LCST.

The core–shell nanoparticles self-assembled from all three of the polymers indeed showed a pH-dependent LCST, which is most likely triggered by the protonation or de-protonation of carboxylic acid groups in the hydrophobic segments of polymers, and is very much influenced by the molar ratio of NIPAAm to DMAAm. In particular, the LCST of the Polymer II nanoparticles is ideal, in view of its value being higher than nominal body temperature in the physiological environment (pH 7.4) but lower than the nominal body temperature in slightly acidic environments. This unique property of the core–shell nanoparticles may be utilized to target drugs to tumor tissues or cell interiors where the environment is characteristically acidic.

Encouraged by the above observations, we focused on Polymer II nanoparticles and their possible application as smart carriers for targeted drug delivery. The hydrophobic microenvironment of Polymer II nanoparticles in water was first investigated by fluorescence spectroscopy using pyrene as a probe. A higher ratio of I_3/I_1 [the intensity (peak height) ratio of the third band (391 nm, I_3) to the first band (371 nm, I_1)] is obtained when pyrene is located in a more hydrophobic environment.[16] This property of pyrene can be utilized to study core–shell nanoparticle formation and deformation. The critical aggregation concentration (CAC) was determined to be approximately $10.0\,\mathrm{mg\,L^{-1}}$ in PBS (pH 7.4). It was noticed that the change in I_3/I_1 after the formation of core–shell nanoparticles was small. This is probably because the core was loosely packed due to the presence of hydrophilic carboxylic groups in the UA segments.

We then investigated the effects of pH and temperature on the size of the blank and doxorubicin (DOX)-loaded core–shell nanoparticles. The blank nanoparticles were prepared by

dissolving Polymer II in dimethylacetamide (DMAc) at a concentration of 0.5 % (w/v), followed by dialysis against 0.02 wt.-% HCl, and 0.02 wt.-% NaOH, respectively, for 24 h using the membrane with a molecular-weight cut-off of 2000 at room temperature. The DOX-loaded nanoparticles were fabricated by a similar protocol. Briefly, 7.5 mg of DOX was neutralized with two moles excess of triethylamine in 3 mL of DMAc and the solution was stirred to dissolve the drug. Fifteen milligrams of polymer was then dissolved in the drug solution. The mixture was then dialyzed against 500 mL of deionized water for 48 h. The DOX-loaded nanoparticles were filtered off and freeze-dried. The actual loading level of DOX in the nanoparticles was about 2.7 % in weight.

The size of the nanoparticles was found to be pH-dependent. In a 0.02 wt.-% HCl solution, the mean diameter of Polymer II nanoparticles was about 319 nm, and in a 0.02 wt.-% NaOH solution, it decreased to about 240 nm. The significantly larger size of the nanoparticles formed in the acidic solution indicates that they contained a higher degree of aggregation due to the greater hydrophobicity of UA at low pH. On the other hand, the repulsion of de-protonated carboxylic acid groups at high pH (pK_a of Polymer II is 6.8) led to a lower degree of aggregation, resulting in a smaller size. The average size of the nanoparticles loaded with DOX was approximately 160–200 nm with a narrow size distribution. From the transmission electron microscopy (TEM) picture (Fig. 2), the size of the DOX-loaded nanoparticles was about 50–60 nm in the solid state, which may be due to the

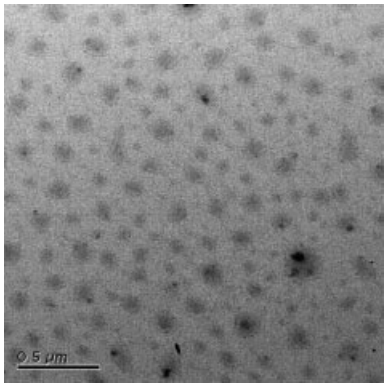

Figure 2. A TEM picture of drug-loaded Polymer II nanoparticles.

collapse of the free hydrophilic segments of the polymer as well as dehydration of the polymer chain. Meanwhile, the nanoparticles were stable in PBS (pH 7.4) at 37 °C (below the LCST). Heating the solution to 40 °C (above the LCST), the size increased to about 988 nm because of aggregation. The aggregates re-dispersed and the size reduced to the original level upon cooling. A similar phenomenon was observed for the nanoparticles at pH 6.6. These results further support the fact that our core–shell nanoparticles were both pH and temperature sensitive, and that the pH and temperature response was reversible.

The stability of the DOX-loaded core–shell nanoparticles was also investigated in PBS (pH 7.4) containing 10 % (w/v) BSA. There was a slight increase in the nanoparticle size (from 104 to 164 nm) after being exposed to BSA for 7 h. This initial size increase might have been due to the hydration of the freeze-dried nanoparticles. After hydration, the size returned to the original and was maintained for the next 3 h. These observations suggest that the presence of proteins in blood would not affect the stability of the nanoparticles.

In-vitro drug release studies of the DOX-loaded nanoparticles were performed under physiological condition (PBS, pH 7.4) and in a slightly acidic environment (pH 6.0 and 6.6) to simulate the pH of the tumor microenvironment. The release profiles of DOX are shown in Figure 3. The drug release from the nanoparticles at pH 7.4 and 37 °C was considerably slow, with an initial burst of about 18%. On the contrary, the

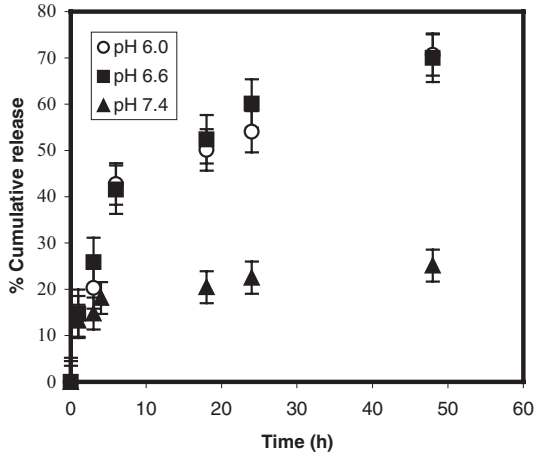

Figure 3. Release profiles of DOX from Polymer II nanoparticles at 37 °C, but at varying pH.

drug release was much faster at pH 6.0 and 6.6 at 37 °C, with approximately 70 % of the drug released within 48 h. In addition, it was observed that the drug-loaded nanoparticles were well dispersed in the buffer at pH 7.4 but aggregated and settled to the bottom of the dialysis bag at pH 6.0 and 6.6. These results corroborate the claim that the nanoparticles are pH sensitive. The change in pH from 7.4 to 6.6 or 6.0 led to the deformation and precipitation of the core–shell nanoparticles, thereby causing the release of the enclosed drug.

The cytotoxicity study of Polymer II was performed using L929 murine fibroblast cells. The cultured cells were exposed to the polymer at concentrations from 10 to 400 mg L^{-1}. Poly(L-lysine) (100 mg L^{-1}) and PEG ($\bar{M}_w$ = 8 kDa, 100 mg L^{-1}) were used as positive and negative controls respectively. Polymer II samples did not display any significant cytotoxicity. Even after 72 h treatment, they still remained less cytotoxic than the positive control.

In summary, the novel Polymer II core–shell nanoparticles synthesized in this study were stable in PBS (pH 7.4) at 37 °C

ADVANCED MATERIALS

but deformed and precipitated in an acidic environment, triggering the release of the enclosed drug molecules. This property may contribute to the selective accumulation of the nanoparticles, as well as the selective release of an encapsulated drug, in acidic tumor tissues or cell interiors. Moreover, the free amine groups on the shell allow further manipulation of the nanoparticles by allowing the attachment of biological signals for targeting.

Experimental

Unless stated otherwise, all reagents and solvents were of commercial grade, and were used as received. *N*-Isopropylacrylamide, *N*,*N*-dimethylacrylamide, and 10-undecenoic acid (98%) were purchased from Aldrich, and were purified by crystallization (*n*-hexane) and reduced-pressure distillation, respectively. The chain-transfer agent (CTA), 2-aminoethanethiol hydrochloride (AET·HCl), was purchased from Sigma–Aldrich. Trinitrobenzene sulfonate (TNBS) as a 1 M aqueous solution was purchased from Fluka. Doxorubicin hydrochloride was kindly provided by Sun Pharmaceuticals, India. 3-[4,5-Dimethylthiazol-2-yl]-2,5-diphenyl tetrazolium bromide (MTT, Duchefa) was used in a 5 mg L^{-1} PBS (pH 7.4) solution for cell quantification. The solution was filtered with a 0.22 μm filter to remove blue formazan crystals.

N-Isopropylacrylamide (3.965 g, 34.99 mmol) and *N*, *N*-dimethylacrylamide (1.48 g, 14.99 mmol) were dissolved in 10 mL of ultra pure water. 10-Undecenoic acid (0.921 g, 5.0 mmol) was converted into its sodium salt by reacting with 5 mL of 4 wt.-% sodium hydroxide solution, and the clear solution of the sodium salt was then added to the *N*-isopropylacrylamide and *N*,*N*-dimethylacrylamide solution. The mixture was purged with purified nitrogen gas for 15 min. APS (0.254 g, 1.11 mmol, 2.0 mol-% of the monomer feed) and AET·HCl (0.244 g, 2.16 mmol, 4.0 mol-% of the monomer feed) were dissolved in 5.0 mL of ultra pure water. This solution was added to the monomer solution slowly with continuous stirring. The reaction was carried out under nitrogen at 27 °C for 48 h. Upon completion, the crude product was precipitated by the addition of excess sodium chloride and dried under vacuum. The precipitate was further dissolved in ethanol, and dialyzed against ultra pure water followed by ethanol using a membrane with a molecular-weight cut-off of 2000 (Spectra/Por). The final product was collected after evaporation of ethanol. The molecular weights of the polymers were determined by gel permeation chromatography (GPC, Waters, polystyrene standards), using THF as the mobile phase (elution rate: 1 mL min^{-1}) at 25 °C. An acid–base titration was performed to estimate the number of carboxylic acid groups and the pK_a of the polymer. Briefly, 100 mg of polymer was dissolved in 10 mL of ultrapure water and titrated with 0.01 N NaOH using phenolphthalein as an indicator. The apparent partition coefficient pK_a of the polymer was also determined by this titration method by continuously measuring the pH during the addition of base. From the graph of pH versus the volume of base, the pK_a was calculated as the pH at half the volume of the base at the equivalence point. The free amine group in the polymer was estimated by spectroscopic determination. A known amount of polymer was dissolved in 2.0 mL of sodium hydrogen carbonate aqueous solution (2.0 %, w/v) containing 0.01 M TNBS. The solution was maintained for 2 h at 40 °C, which was then cooled and diluted to a specific volume. The amount of amine functional groups derivatized with TNBS in the sample was determined using a UV-vis spectrophotometer (UV-2501PC, Shimadzu) at 345 nm using alanine as a standard [17]. The experiments were performed in triplicate and the average values were presented.

The Determination of the CAC of Polymer II: Aliquots of pyrene solutions (1.54×10^{-5} M in acetone, 400 mL) were added to 10 mL volumetric flasks, and the acetone was allowed to evaporate. Polymer solutions at concentrations ranging from 1.0×10^{-5} to 1.0 g L^{-1} were prepared in PBS (pH 7.4). The aqueous polymer solutions (10 mL) were then added to the volumetric flasks containing the pyrene residue. All the sample solutions contained excess pyrene content at the same concentration of 6.16×10^{-7} M. The solutions were allowed to equilibrate for 24 h at room temperature (20 °C). Fluorescence spectra of the polymer solutions were then recorded on an LS50B luminescence spectrometer (Perkin Elmer, USA) at room temperature. The emission spectra were recorded from 350 to 500 nm with an excitation wavelength of 340 nm. Both excitation and emission bandwidths were set at 5 nm. From the pyrene emission spectra, the intensity (peak height) ratio (I_3/I_1) of the third band (391 nm, I_3) to the first band (371 nm, I_1) was analyzed as a function of polymer concentration. The CAC value was taken from the intersection of the tangent to the curve at the inflection with the horizontal tangent through the points at low concentrations. The experiments were conducted in triplicate and the average values were reported. The size of the core–shell nanoparticles was analyzed using ZetaPals (Brookhaven Instruments Corporations, CA, USA) equipped with a He–Ne laser beam (670 nm). Each measurement was repeated five times, and was found to be in good agreement. The morphology of the core–shell nanoparticles was analyzed by TEM. A drop of the freshly prepared nanoparticle solution containing 0.01 % (w/v) phosphotungstic acid was placed on a copper grid coated with a polymer film, and was air-dried at room temperature. The TEM observations were carried out on a JEM-2010 microscope with an electron kinetic energy of 200 keV.

In-Vitro Release of DOX: A certain amount of DOX-loaded freeze-dried nanoparticles was dispersed in 200 μL of the respective buffer solution and allowed to stabilize for 30 min before being placed in a dialysis membrane with a molecular-weight cut-off of 2000 (Spectra/Por). The dialysis bag was then immersed in 25 mL of PBS at pH 6.0, 6.6, or 7.4 at 37 °C. The samples were drawn at specific time intervals and the drug concentration was analyzed using a UV-vis spectrophotometer at 485 nm. The drug loading was calculated based on the standard curve obtained from DOX in the buffers. The in-vitro release experiments were carried out in triplicate for each pH.

Cytotoxicity Study: Polymer solutions were prepared at stock concentrations. These solutions were sterilized with 0.22 μm syringe filters and diluted with PBS (pH 7.4) and growth media to give the polymer at final concentrations of 10, 100, 300, and 400 mg L^{-1} (ppm). Poly(L-lysine) and PEG ($\bar{M}_w$ 8 kDa) at a concentration of 100 ppm were used as the positive and negative controls, respectively. The L929 mouse fibroblast cells were cultured in supplemented Dulbecco's Modified Eagles Medium (DMEM; 10 % fetal bovine serum, 1 % L-glutamate, 1 % penicillin-streptomycin) (GibcoBRL) and incubated at 37 °C, under 5 % CO_2. The cells were seeded onto 96-well plates at 10 000 cells per well. The plates were then returned to the incubator and the cells were allowed to grow to confluence. On the morning of the initiation of the tests, the media in the wells were replaced with 150 μL of the pre-prepared growth medium sample mixture. The plates were then returned to the incubator and maintained in 5 % CO_2, at 37 °C, for 24, 48, and 72 h. The mixture in each well was replaced with fresh aliquots every morning for the exposure period. Each sample was tested in eight replicates per plate. Three plates were used for each period of exposure, making a total of 24 replicates per sample. Fresh growth media and 20 μL aliquots of MTT solution were used to replace the mixture in each well after the designated period of exposure. The plates were then returned to the incubator and maintained in 5 % CO_2, at 37 °C, for a further 3 h. The growth medium and excess MTT in each well were then removed. Dimethyl sulfoxide (150 μL) was then added to each well to dissolve the internalized purple formazan crystals. An aliquot of 100 μL was taken from each well and transferred to a fresh 96-well plate. The plates were then assayed at 550 and 690 nm. The absorbance readings of the formazan crystals were taken to be that at 550 nm subtracted by that at 690 nm. The results were expressed as a percentage of the absorbance of the blank, which comprised PBS of a comparative volume, added to the growth medium.

Received: July 3, 2004
Final version: September 15, 2004

[1] K. Kataoka, A. Harada, Y. Nagasaki, *Adv. Drug Delivery Rev.* **2001**, *47*, 113.
[2] V. P. Torchilin, *J. Control. Rel.* **2001**, *73*, 137.
[3] F. Liu, A. Eisenberg, *J. Am. Chem. Soc.* **2003**, *125*, 15 059.
[4] Y. Matsumura, H. Maeda, *Cancer Res.* **1986**, *46*, 6387.
[5] A. V. Kabanov, V. P. Chekhonin, V. Y. Alakhov, E. V. Batrakova, A. S. Lebedev, N. S. Melik-Nubarov, S. A. Arzhakov, A. V. Levashov, G. V. Morozov, E. S. Severin, V. A. Kabanov, *FEBS Lett.* **1989,** *258*, 343.
[6] J. E. Chung, M. Yokoyama, M. Yamato, T. Aoyagi, Y. Sakurai, T. Okano, *J. Controlled Release* **1999**, *62*, 115.
[7] P. W. Vaupel, S. Frinak, H. I. Bicher, *Cancer Res.* **1981**, *41*, 2008.
[8] D. C. Drummond, M. Zignani, J. C. Leroux, *Progr. Lipid Res.* **2000**, *39*, 409.
[9] E. S. Lee, H. J. Shin, K. Na, Y. H. Bae, *J. Controlled Release* **2003**, *90*, 363.
[10] E. S. Lee, K. Na, Y. H. Bae, *J. Controlled Release* **2003**, *91*, 103.
[11] M. Yamato, M. Utsumi, A. Kushida, C. Konno, A. Kikuchi, T. Okano, *Tissue Eng.* **2001**, *7*, 473.
[12] G. Chen, A. S. Hoffman, *Nature* **1995**, *373*, 49.
[13] C. S. Chaw, K. W. Chooi, X. M. Liu, D. Tan, L. Wang, Y. Y. Yang, *Biomaterials* **2004**, *25*, 4297.
[14] G. Bokias, A. Durand, D. Hourdet, *Macromol. Chem. Phys.* **1998**, *199*, 1387.
[15] Y. Katsumoto, T. Tanaka, H. Sato, O. Yukihiro, *J. Phys. Chem. A.* **2002**, *106*, 3429.
[16] D. C. Dong, M. A. Winnik, *Can. J. Chem.* **1984**, *62*, 2560.
[17] S. Syder, P. Sobocinski, *Anal. Biochem.* **1975**, *64*, 284.

Rapid Functionalization of Mesoporous Materials: Directly Dispersing Metal Oxides into As-Prepared SBA-15 Occluded with Template**

By *Yi Meng Wang*, *Zheng Ying Wu*, *Li Ying Shi*, and *Jian Hua Zhu**

The unique surface and pore structure of ordered mesoporous materials make them promising for applications in adsorption and catalysis. However, siliceous mesoporous materials usually suffer from a lack of active sites necessary for adsorption or catalysis, and thus their functionalization becomes paramount for application in industry. This is achieved by incorporating guest species such as metals or metal oxides by direct synthesis (one-pot method) or post-modification after synthesis. In the latter process, the host template is removed by either calcination or extraction to achieve an open-porous structure prior to functionalization, in which the thermal transformation of the precursor into the final oxide guest is critical. In order to save energy and time, it is better to remove the template and to transform the guest precursor in one calcination step in order to modify the as-prepared mesoporous materials. This was attempted recently with guest species replacing surfactants in solution, where surfactant extraction releases some space for the surface modification.[1–3]

Here, we report a new solvent-free method for directly inserting guest precursors into the occluded pores of as-prepared ordered mesoporous materials followed by calcination, thus preparing a mesoporous functional composite with unexpectedly high oxide dispersion. This new strategy is not only energy- and time-efficient, but also sheds light on how to exploit the confined space between the templated aggregates and the silica walls.

Thermogravimetric analysis (TGA) showed 41 % weight loss in the range of 423–823 K for as-prepared SBA-15 samples, and 45 % and 41 % weight loss for as-prepared MCM-41 samples M1 and M2, respectively, due to decomposition of the template species. (As described in the Experimental section, M1 is prepared under acidic conditions, and M2 is prepared under alkaline conditions.) Although these data are slightly lower than previously reported values[4,5] (e.g., a decomposition weight loss of about 46 % observed for SBA-15[4]), this means that most of the templated aggregates still occlude the pores of both these as-prepared samples, and that less than 15 % of the pore volume is available for the dispersion of a guest. However, an unexpectedly high dispersion of metal-oxide species can be realized in the mesoporous support by this new method. When the as-prepared SBA-15 was used as a support, no reflections of the CuO crystalline phase were visible in the wide-angle X-ray diffraction (XRD) patterns, even for the CuO/SBA-15(20) composite (Fig. 1A). (The samples are denoted as MO_n/Support(X), where MO_n represents the metal-oxide species and X is the weight percentage of MO_n in the composites.) That is, about 40 wt.-% of $Cu(NO_3)_2$ has been spontaneously dispersed in the host and transformed to copper oxide. As shown in Figure 1B, low-angle XRD patterns of all the calcined CuO/SBA-15 composites (with weight percentages of 15 wt.-%, 20 wt.-%, and 25 wt.-%) are identical to that of SBA-15, with two-dimensional hexagonal pore ordering corresponding to a *p6mm* space group. Even at the highest weight percent of CuO (25 wt.-%), there was still no CuO crystalline phase seen in the wide-angle XRD pattern. However, as revealed by ultraviolet diffuse-reflectance spectroscopy (DRS, Fig. 2), small CuO_x clusters begin to aggregate, forming the shoulder of a charge-transfer band at ~320 nm.[6,7] On the other hand, the composite prepared by this new method possesses an improved mesostructure: CuO/SBA-15(10) has a larger surface area (579 $m^2 g^{-1}$) and pore volume (0.78 $cm^3 g^{-1}$) than the corresponding sample fabricated by the traditional wet impregnation of template-free SBA-15 (surface area of 482 $m^2 g^{-1}$ and pore volume of 0.73 $cm^3 g^{-1}$). Both CuO/SBA-15(10) samples

[*] Prof. J. H. Zhu, Y. M. Wang, Z. Y. Wu, L. Y. Shi
Key Laboratory of Mesoscopic Chemistry, Department of Chemistry
Nanjing University
Nanjing 210093 (P. R. China)
E-mail: jhzhu@netra.nju.edu.cn

[**] This work was supported by NSF of China (20273031 and 20373024), Ningbo Cigarette Factory, and Analysis Center of Nanjing University. We thank C. F. Zhou for help with drawing the schematic diagram.

DOI: 10.1002/adma.200400860